Cellular and Molecular Life Sciences (2021) 78:3591–3606
https://doi.org/10.1007/s00018-020-03754-x

ORIGINAL ARTICLE

Ribosomal protein S3 associates with the TFIIH complex and positively regulates nucleotide excision repair

Y. J. Park[1] · S. H. Kim[1] · T. S. Kim[1] · S. M. Lee[1] · B. S. Cho[1] · C. I. Seo[1] · H. D. Kim[2] · J. Kim[1,2]

Received: 23 January 2020 / Revised: 14 December 2020 / Accepted: 29 December 2020 / Published online: 19 January 2021

Abstract

In mammalian cells, the bulky DNA adducts caused by ultraviolet radiation are mainly repaired via the nucleotide excision repair (NER) pathway; some defects in this pathway lead to a genetic disorder known as xeroderma pigmentosum (XP). Ribosomal protein S3 (rpS3), a constituent of the 40S ribosomal subunit, is a multi-functional protein with various extra-ribosomal functions, including a role in the cellular stress response and DNA repair-related activities. We report that rpS3 associates with transcription factor IIH (TFIIH) via an interaction with the xeroderma pigmentosum complementation group D (XPD) protein and complements its function in the NER pathway. For optimal repair of UV-induced duplex DNA lesions, the strong helicase activity of the TFIIH complex is required for unwinding damaged DNA around the lesion. Here, we show that XP-D cells overexpressing rpS3 showed markedly increased resistance to UV radiation through XPD and rpS3 interaction. Additionally, the knockdown of rpS3 caused reduced NER efficiency in HeLa cells and the overexpression of rpS3 partially restored helicase activity of the TFIIH complex of XP-D cells in vitro. We also present data suggesting that rpS3 is involved in post-excision processing in NER, assisting TFIIH in expediting the repair process by increasing its turnover rate when DNA is damaged. We propose that rpS3 is an accessory protein of the NER pathway and its recruitment to the repair machinery augments repair efficiency upon UV damage by enhancing XPD helicase function and increasing its turnover rate.

Keywords rpS3 · TFIIH · Extra-ribosomal function · NER · XPD

Abbreviations

CPD	Cyclobutane pyrimidine dimer
NER	Nucleotide excision repair
rpS3	Ribosomal protein S3
TFIIH	Transcription factor IIH
XP	Xeroderma pigmentosum

Introduction

Cells are under constant attack by various agents that generate DNA damages, which, if unrepaired, can lead to mutations as well as genomic instability and cell death or tumorigenesis [1]. Among the various causes of DNA damage, ultraviolet (UV) radiation, which is abundant in sunlight, causes structural aberrations in DNA, including 6–4 photoproducts (6-4PPs), cyclobutane pyrimidine dimers (CPDs), and inter/intra-strand DNA crosslinks [2]. Cells are equipped with an array of specific mechanisms to repair and minimize any debilitating effects of DNA damage [3–5]. In mammalian cells, bulky DNA lesions like CPDs caused by UV irradiation are usually repaired by nucleotide excision repair (NER), which is a complex, multi-step process involving many proteins. In NER, after various surveillance proteins sense and confirm damage [6], transcription factor IIH (TFIIH) is recruited to the damaged DNA [7] and, upon confirmation of a lesion, it creates a "bubble" around the lesion by utilizing its ATPase/DNA helicase activities [8, 9]. Two DNA endonucleases, XPG and XPF, remove the short stretch of DNA

Electronic supplementary material The online version of this article (https://doi.org/10.1007/s00018-020-03754-x) contains supplementary material, which is available to authorized users.

✉ J. Kim
joonkim@korea.ac.kr

[1] Lab of Biochemistry, Division of Life Sciences, Korea University, Seoul 02841, Korea

[2] TechnoComplex Building, HAEL Lab, Korea University, Seoul 02841, Korea

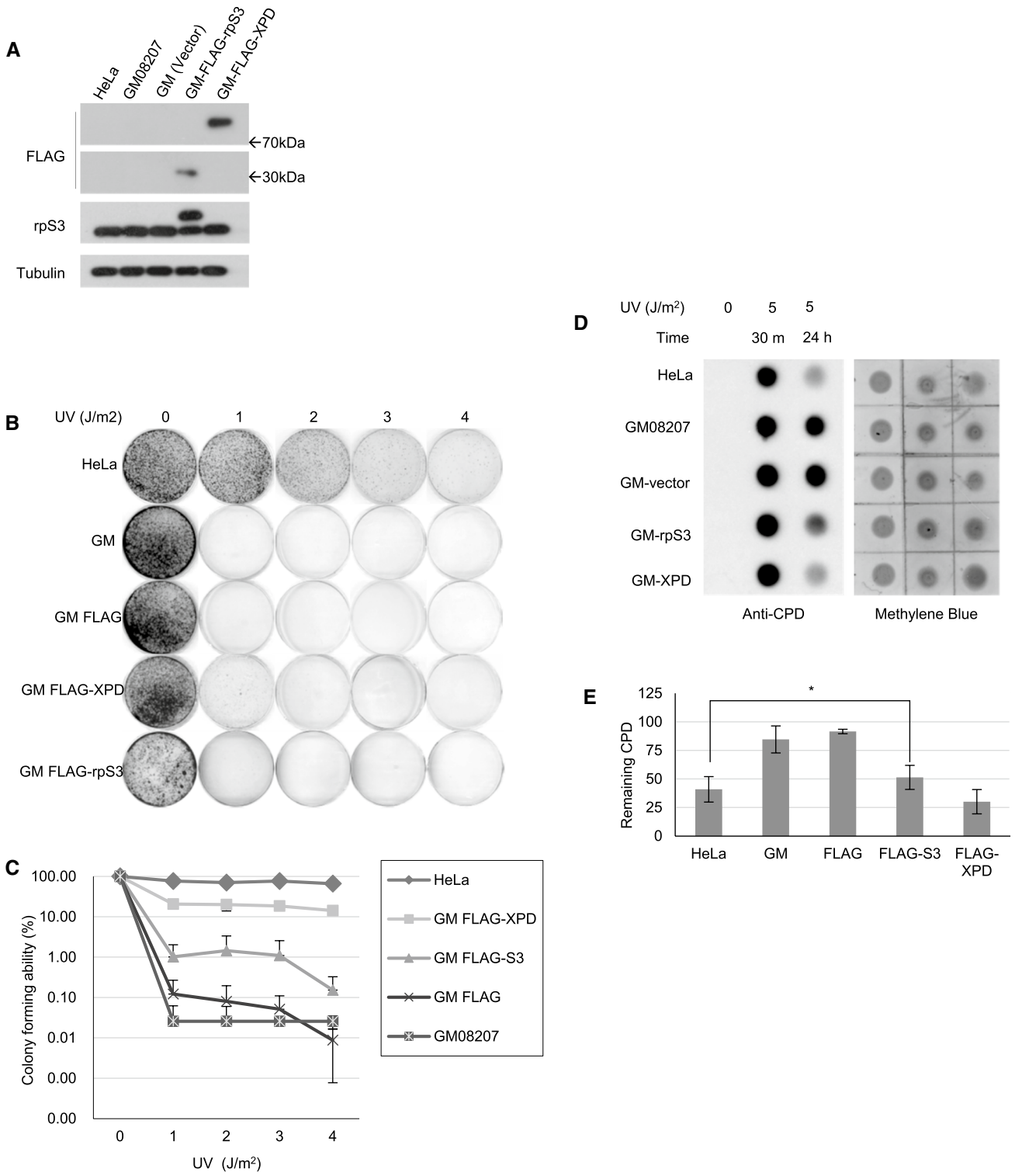

strand containing damages [10, 11]. Finally, the resulting gap formed in the DNA, which is approximately 33 nucleotides (nt) long, is filled in by DNA polymerase and ligase [11]. Successful NER cannot be achieved if one part of the NER machinery is defective. Defects in the NER machinery are associated with several serious hereditary diseases, including xeroderma pigmentosum (XP), Cockayne syndrome (CS), and trichothiodystrophy (TTD) [12, 13]. Patients with these diseases usually exhibit severely reduced NER activities and hypersensitivity toward UV light [14].

◂**Fig. 1** Overexpression of rpS3 confers UV resistance to GM08207 XP-D cells. **a**–**e** GM08207 XP-D cells were transfected with the FLAG-tagged empty plasmid vector (GM-FLAG), plasmid with FLAG-tagged XPD (GM-FLAG-XPD) or FLAG-tagged rpS3 (GM-FLAG-S3), and the expression level of FLAG-tagged proteins were checked using western blot (**a**). (**b**, **c**) The transfected cells were irradiated with UV-C with indicated doses. After 7 days, cells were fixed and stained with crystal violet dye to count colonies (**b**). Colony-forming abilities are represented as the averages of the percent of colonies formed by an unirradiated control. Data are from three separate experiments (**c**). Errors bars represent standard deviations. Y-axis is in a logarithmic scale with factor of 10. **d**, **e** The transfected cells were irradiated with 0 or 5 J/m^2 of UV-C and incubated for the indicated times. Genomic DNA was extracted from cells, 2 μg of DNA was dot-blotted, and immunoblotting was performed with anti-CPD monoclonal antibody. Percentage of unrepaired CPD (the ratio of remaining CPD in 24 h to 30 min after UV-C treatment) were shown as a graph in (**e**). Error bars represent standard deviations (*: p value < 0.05)

Ribosomal protein S3 (rpS3) is a member of the 40S small ribosomal subunit, and, besides its basic role as part of the ribosome's translational machinery, it has extra-ribosomal functions; rpS3, also known as UV endonuclease III, cleaves DNA with abasic (AP) sites and thymine glycol lesions generated by UV damage so that it participates in basic excision repair (BER) [15, 16]. rpS3 is reported to be involved in AP DNA processing in eukaryotic cells [17, 18]. Also, treatment with exogenous rpS3 provides protection of mouse skin cells against UV irradiation [19, 20]. Additionally, rpS3 is involved in the oxidative stress-induced mitochondrial DNA damage response in mammalian cells [21]. In addition to these DNA repair-related functions, rpS3 participates in the stress response and cell cycle control [22], involved in protein quality control and ribosomal stress response [23, 24], and can induce apoptosis through JNK activation by its association with TRADD [25]. Also, rpS3 is reported to be associated with NM23-H1 and reduces the rate of metastasis via inhibition of ERK pathway and MMP-9 secretion [26]. Furthermore, rpS3 interacts with NF-κB to participate in the non-canonical NF-κB pathway during bacterial infections [27, 28]. These reports suggest a role of rpS3 as a cellular regulator that fine-tunes various processes involved in DNA damage and stress responses.

In this study, we present a novel role of rpS3 in the NER pathway. Through its upregulation and association with the TFIIH complex, rpS3 increases the efficiency of UV damage repair. Higher expression of rpS3 confers increased resistance to UV irradiation in the XP-D patient-derived cell strain. We show that rpS3 is a helper protein of the NER machinery, augmenting its repair activity by accelerating the turnover rate of its core complex.

Results

RpS3 overexpression increases UV resistance in GM08207 XP-D cells

XP patients are severely sensitive to UV light due to defective NER. To investigate the possible role of rpS3 in UV-induced DNA damage processing, we performed a colony-forming assay and MTT assay. The GM08207 XP-D cell line, which is a transformed human fibroblast cell line derived from an XPD patient, has a point mutation in the XPD gene (ERCC2) at the arginine 683 (R683) residue that converted into tryptophan (R683W) and severely reduces the helicase activity of the XPD protein. We transiently transfected XP-D cells with an empty vector, plasmids expressing FLAG-tagged rpS3, or FLAG-tagged wild-type XPD protein (Fig. 1a), followed by irradiation with UV-C from 1–4 J/m^2 and incubated for 7 days until the appearance of colonies. HeLa cells were used as a wild-type XPD control. Colonies were counted for each set, and colony formation was expressed as the relative percentage to unirradiated cells (Fig. 1b). As expected, XP-D cells transfected with wild-type XPD protein (GM FLAG-XPD) showed markedly increased UV-resistance compared to the control cells (GM08207). Interestingly, we found that cells overexpressing rpS3 (GM FLAG-S3), while not as much as XP-D cells expressing wild-type XPD, have also increased resistance to UV radiation compared to the control cells. We also exposed cells with 5 J/m^2 of UV-C and tracked cell survival rates using an MTT (3-(4,5-dimethylthiazol-2-yl)-2,5-diphenyltetrazolium bromide)-formazan assay (Supplementary Fig. 1). In agreement with the results shown in Fig. 1b, both XP-D cells expressing wild-type XPD protein and the cells overexpressing rpS3 exhibited increased cell survival after UV irradiation compared to control cells. These results reveal that the UV resistance of XP-D cells was enhanced by the expression of wild-type XPD or rpS3; while not as much as the wild-type XPD protein does, rpS3 overexpression in XP-D cells moderately increased cell survival after UV irradiation.

rpS3 is involved in NER

As the rapid repair of UV-induced DNA damage via the NER pathway is key to UV resistance and cell survival, we investigated the possibility of rpS3 involvement in NER. We performed a genomic DNA dot blot assay against anti-CPD antibody (Fig. 1c, d). We transfected GM08207 cells with an empty vector, a vector bearing FLAG-tagged rpS3, or wild-type XPD. HeLa cells were

also used as a positive control. After exposing each cell type to 5 J/m^2 UV-C radiation, cells were incubated up to 24 h to allow processing and repair of UV-induced damage. Then, the genomic DNA was extracted and subjected to dot blot analysis using an anti-CPD antibody to measure the remaining unrepaired lesions. Twenty-four hours after irradiation, XP-D cells overexpressing the wild-type XPD protein had improved UV damage repair capability in comparison to cells expressing the empty vector. Cells overexpressing FLAG-rpS3, while not as much as the cells transfected with wild-type XPD, showed an increase in UV damage removal compared to control cells. This result agrees with the Fig. 1b and suggests that rpS3 is involved in the UV-damage repair mechanism.

To further confirm the involvement of rpS3 in UV damage processing, we treated cells with rpS3-specific siRNAs (Fig. 2a) and measured cell survival using the MTT assay. The result revealed that HeLa cells transfected with si-rpS3 have reduced resistance to UV damage compared to control cells (Fig. 2b). Furthermore, we examined processing kinetics using the alkaline comet assay (Fig. 2c). As an essential step of the NER process, approximately 27 to 33 nucleotides (nts) long DNA single strands containing UV lesions (CPD or 6-4PP) must be excised by XPF and XPG nucleases, therefore generating temporary single-strand chromosomal gaps [29]. These can be studied by the alkaline comet assay to reveal the transient ssDNA intermediates created during the NER process [30], thus, indirectly measuring the rate

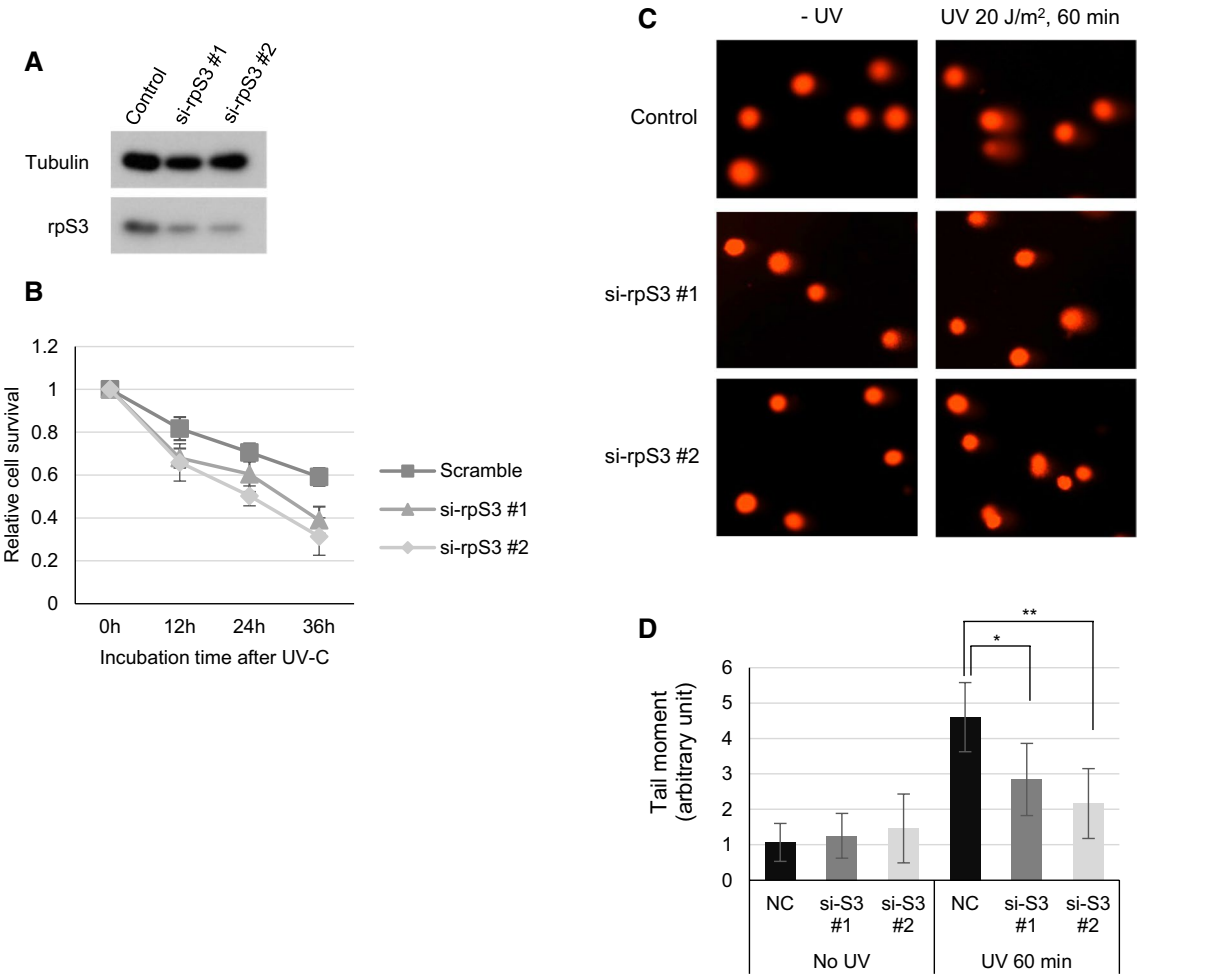

Fig. 2 Knockdown of rpS3 in HeLa cells increases UV sensitivity and decreases CPD repair. **a**, **b** HeLa cells were transfected with 10 pmol of either scrambled or two rpS3-specific siRNAs each targeting different sequences and harvested after 24 h. Cell lysates were immunoblotted with anti-rpS3 antibody. Anti-tubulin antibody was used as an internal control (**a**). The siRNA transfected cells were irradiated with 5 J/m^2 of UV-C and incubated for the indicated amounts of time. Cells were then subjected with MTT assay; relative cell survivals are averages of fold absorbance at 595 nm relative to the absorbance of unirradiated controls. Error bars represent standard deviations (**b**). **c**, **d** HeLa cells transfected with scrambled or two rpS3 siRNAs were irradiated with 20 J/m^2 of UV-C after 24 h post-transfection, incubated in 37 °C, and harvested after 60 min. Cells were embedded in low-gelling point agarose, and an alkaline comet assay was performed (**c**). The tail moment was calculated using CometScore Software (Tritek Corp.), and results are shown as a graph in (**d**). (*, **: p value < 0.05)

of UV-damaged DNA processing via NER machinery—the more robust NER, the more the ssDNA gaps are generated. HeLa cells were transfected with either scrambled siRNA or two siRNAs specific to rpS3 (Fig. 2a), and, after 24 h, cells were UV-C irradiated with 20 J/m^2. Cells were gently harvested with 0.05% Trypsin–EDTA, and the alkaline comet assay was performed (Fig. 2c). Cells with reduced rpS3 expression showed a significant decrease in the tail moment (Fig. 2d), indicating a reduced damage processing rate compared to control cells. In line with the previous results, knockdown of rpS3 caused reduced tail moments after UV exposure, implying that rpS3 has a role in the NER pathway as knockdown of rpS3 caused reduced NER efficiency. These results demonstrate that rpS3 is involved in the rapid processing of UV-induced lesions and its knockdown impairs DNA damage removal in vitro.

rpS3 associates with the TFIIH complex

As rpS3 overexpression confers UV resistance to XP-D cells and knockdown of rpS3 resulted in decreased DNA damage processing, we examined the molecular interactions between rpS3 and core NER machinery, TFIIH. We performed a co-immunoprecipitation assay using antibodies specific to XPD and XPB, which are the two core components of TFIIH, and found that rpS3 was interacting with the TFIIH complex proteins (Fig. 3a). Reciprocally, immunoprecipitation using an rpS3 antibody also showed that rpS3 associates with XPD and XPB proteins (Fig. 3b). Furthermore, the interaction between XPD and rpS3 appeared to increase after UV-irradiation (Fig. 3c). It is reported that the C-terminal domain of XPD, which contains a helicase domain, is responsible for most XPD diseases and the R683W mutation, in particular, is frequently found in XPD patients [31], including GM08207 cells used in this study. To investigate whether the interaction between rpS3 and XPD was altered in cells with an XPD phenotype, we compared the levels of interaction between rpS3 and XPD using wild-type cells and XP-D phenotype cells using co-IP (Fig. 3d). GM08207 cell, which contains R683W mutant XPD protein, has markedly reduced interaction with rpS3. Also, we co-transfected 293 T cells with FLAG-S3 with GFP-tagged wild-type XPD or GFP-XPD R683W and performed co-immunoprecipitation assay using anti-FLAG antibody and subsequently immunoblotted with anti-GFP antibody or anti-FLAG antibody (Fig. 3e). In both experiments, the R683W mutant XPD proteins were still able to interact with rpS3, but the interaction of the wild-type XPD protein with rpS3 was stronger. This result suggests the possibility of an interaction between the C-terminal helicase domain of XPD and rpS3. Additionally, using immunofluorescence and micropore UV-irradiation assay ([32, 33]), we visualized the interaction between rpS3 and XPD protein via fluorescence microscopy. Cells were irradiated with 100 J/m^2 of UV-C through a 2 μm isopore polycarbonate filter to induce localized lesions within the nucleus, and after 60 min, cells were fixed and incubated with rpS3 and XPD- and XPB-specific antibodies. We found that after micropore UV irradiation, rpS3 formed foci with XPD and XPB within the nucleus, indicating that rpS3 indeed interacts with UV-damage repair foci within the nucleus (Fig. 3f).

To further confirm the presence of rpS3 in the NER repair complex, we performed an electrophoretic mobility shift assay (EMSA) using a DNA probe containing a UV-damaged lesion. To use as a substrate, we designed a 110-bp stretch of DNA with a single *EcoR*I restriction enzyme site at the center (Fig. 4a). The substrate DNA was irradiated with 500 J/m^2 of UV-C to induce thymine dimer formation at the *EcoR*I site, and results showed that *EcoR*I was not able to cleave the DNA due to the presence of cyclobutane UV damage at the two thymidine residues within the restriction site (Fig. 4b, c). We radiolabeled the UV-irradiated and unirradiated DNA substrates at the 5′ end with [γ-^{32}P] ATP and mixed them with the cell-free extract from HeLa cells. The shifted band (complex 1) only appeared in the mixture of UV-irradiated DNA fragments (Fig. 4d), and its intensity increased as more cell-free extracts were added. Complex 1 disappeared when the non-radiolabeled, UV-irradiated substrate (cold competitor) was added (Fig. 4e), showing that complex 1 is indeed a DNA–protein complex, which specifically binds to UV-damaged DNA. To identify whether complex 1 contains both of XPD and rpS3, a supershift assay was performed (Fig. 4f). The cell-free extract from the pcDNA-FLAG-XPD-transfected HeLa cells was mixed with the damaged DNA probe and anti-FLAG or anti-rpS3 antibodies. The supershifted bands (complex 2) in lanes 1 and 3 of Fig. 4f demonstrated that complex 1 contained XPD and rpS3. Additionally, to illustrate the influence of mutant XPD on the association of rpS3 to damaged DNA, pcDNA-FLAG-XPD R683W was also transfected into HeLa cells. As shown in lane 4 of Fig. 4f, mutant XPD still interacted with damaged DNA, but the interaction with rpS3 (lane 6) was weaker than that of the wild type (lane 3). These results show that rpS3 and XPD interact along CPD-containing DNA, strongly implying that they work cooperatively to repair damaged DNA. Also, the interaction of these proteins appears to occur only on CPD-containing DNA. While the binding affinity of mutant XPD to CPD-containing DNA was comparable to that of wild-type XPD, rpS3 binding to CPD-containing DNA was stronger in the presence of wild-type XPD than with mutant XPD. This suggests that the interaction between rpS3 and TFIIH is dependent on XPD and the mutation of XPD's helicase domain weakens interaction between XPD and rpS3.

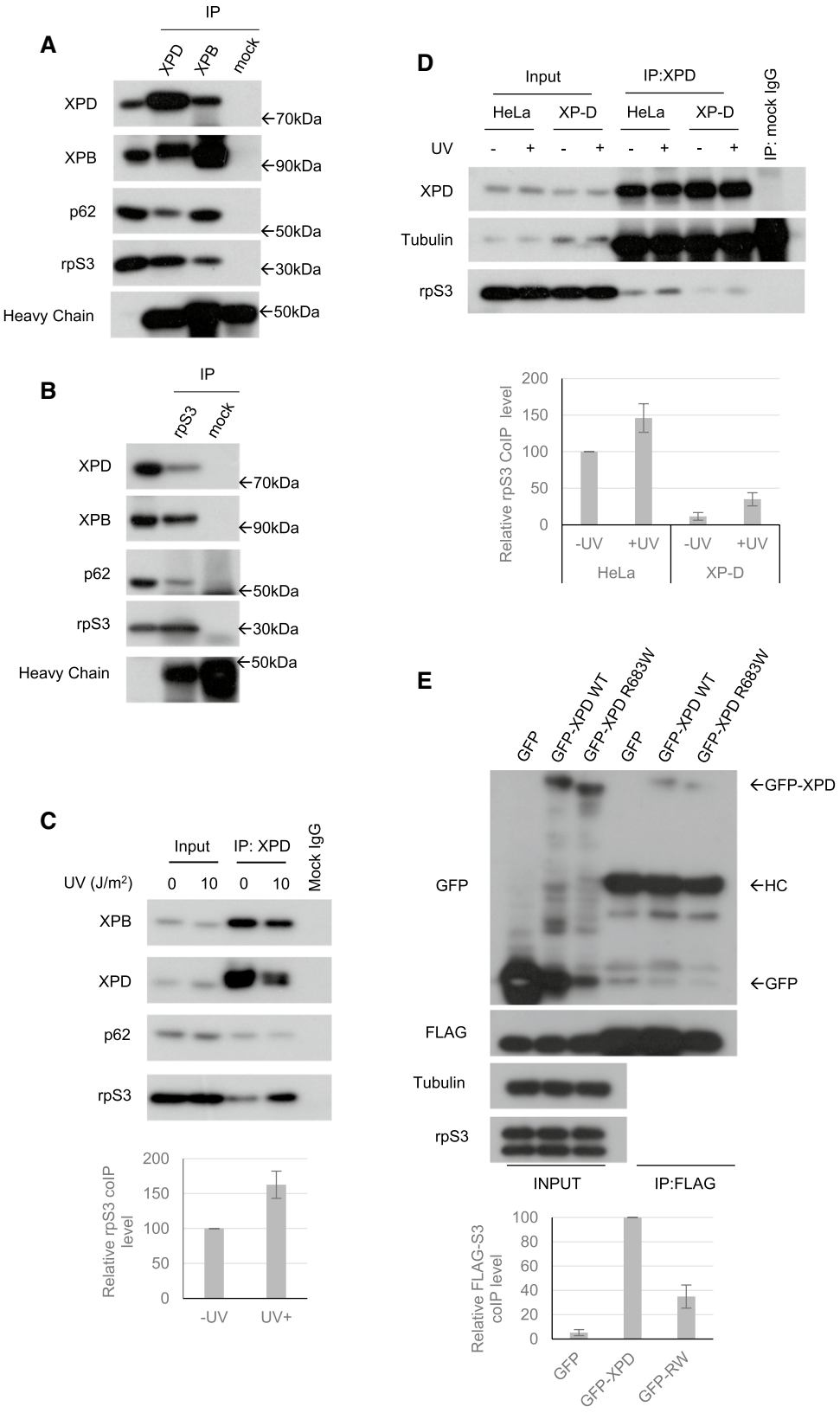
A
IP
XPD
XPB
mock
XPD
XPB
p62
rpS3
Heavy Chain
←70kDa
←90kDa
←50kDa
←30kDa
←50kDa
B
IP
rpS3
mock
XPD
XPB
p62
rpS3
Heavy Chain
←70kDa
←90kDa
←50kDa
←30kDa
←50kDa
C
Input
IP: XPD
Mock IgG
UV (J/m²)
0
10
0
10
XPB
XPD
p62
rpS3
Relative rpS3 coIP level
200
150
100
50
0
-UV
UV+
D
Input
IP:XPD
IP: mock IgG
HeLa
XP-D
HeLa
XP-D
UV
- + - + - + - +
XPD
Tubulin
rpS3
Relative rpS3 CoIP level
200
150
100
50
0
-UV
+UV
-UV
+UV
HeLa
XP-D
E
GFP
GFP-XPD WT
GFP-XPD R683W
GFP
GFP-XPD WT
GFP-XPD R683W
←GFP-XPD
←HC
←GFP
GFP
FLAG
Tubulin
rpS3
INPUT
IP:FLAG
Relative FLAG-S3 coIP level
100
80
60
40
20
0
GFP
GFP-XPD
GFP-RW

◀ **Fig. 3** rpS3 interacts with XPD. **a** Nuclear extract (500 μg) from HeLa cells was immunoprecipitated (IP) with anti-XPB antibody, anti-XPD antibody, and normal mouse IgG as a control. The IP fraction was immunoblotted with anti-XPB, anti-XPD, anti-p62, and anti-rpS3 antibodies. Molecular weight is indicated with arrows. **b** Nuclear extract (500 μg) obtained from HeLa cells was immunoprecipitated with anti-rpS3 antibody and normal rabbit IgG. The IP fraction was immunoblotted with anti-XPB, anti-XPD, and anti-rpS3 antibodies. **c** HeLa cells were irradiated with 10 J/m2 of UV-C, and after 1 h, cells were harvested, and nuclear fractions were isolated. Co-IP assay using XPD antibody was performed with nuclear extracts from unirradiated and radiated cells, and IP fraction was immunoblotted with antibodies indicated (upper panel). Co-IP level of rpS3 was quantified from triplicate experiments and shown here as a graph (lower panel). **d** Using HeLa cells and GM08207 XP-D cells, co-IP assay was performed with anti-XPD antibodies. Cells were irradiated with 10 J/m2 of UV-C, and after 1 h, cells were harvested and whole cell lysates were collected. With each lysate, co-immunoprecipitation assay was performed using anti-XPD antibody (upper panel). Co-IP level of rpS3 of each sample was quantified from triplicate experiments and shown as a graph (lower panel). **e** pcDNA FLAG-S3 was co-transfected with pEGFP-C1(GFP), pEGFP-XPD(XPD), or pEGFP-XPD R683W(R683W) into 293 T cells. Transfected 293 T cell lysate was immunoprecipitated with anti-FLAG antibody. Input and IP fractions were subsequently immunoblotted with anti-FLAG antibody and anti-GFP antibody. The resulting bands are indicated by arrows (upper panel). The amount of interaction between FLAG-rpS3 and GFP-tagged proteins from three separate experiments was quantified and shown as a graph (lower panel). **f** HeLa cells were covered with 2 μm polycarbonate isopore filter and irradiated with 100 J/m^2 of UV-C to induce localized UV-damage foci in the nucleus and fixed after 60 min using formaldehyde. Cells were incubated with anti-rpS3, anti-XPD, or anti-XPB antibodies and appropriate fluorescence-conjugated secondary antibodies. Cells were then visualized with immunofluorescence using a Carl Zeiss AXIO Z1 fluorescence microscope

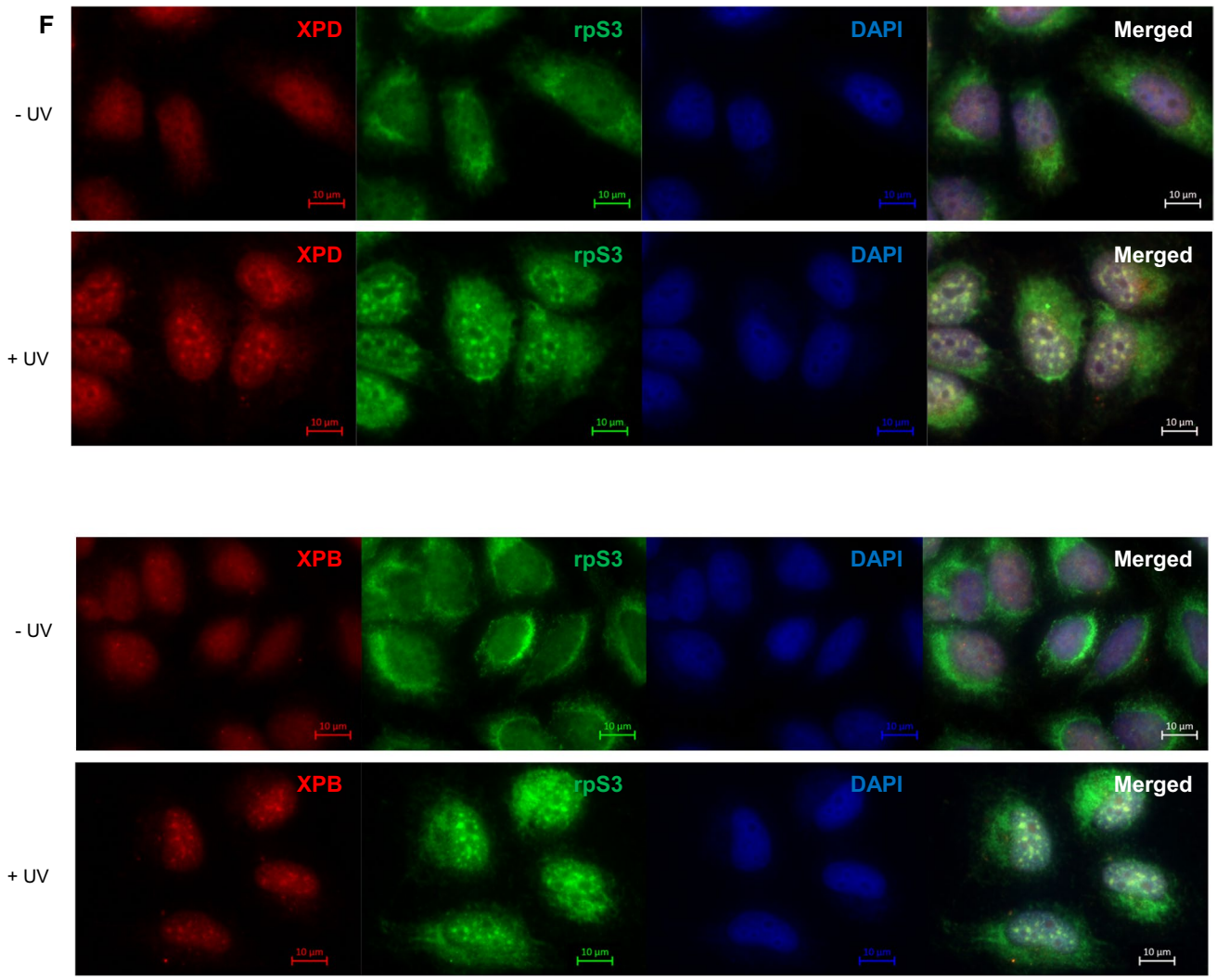

Fig. 3 (continued)

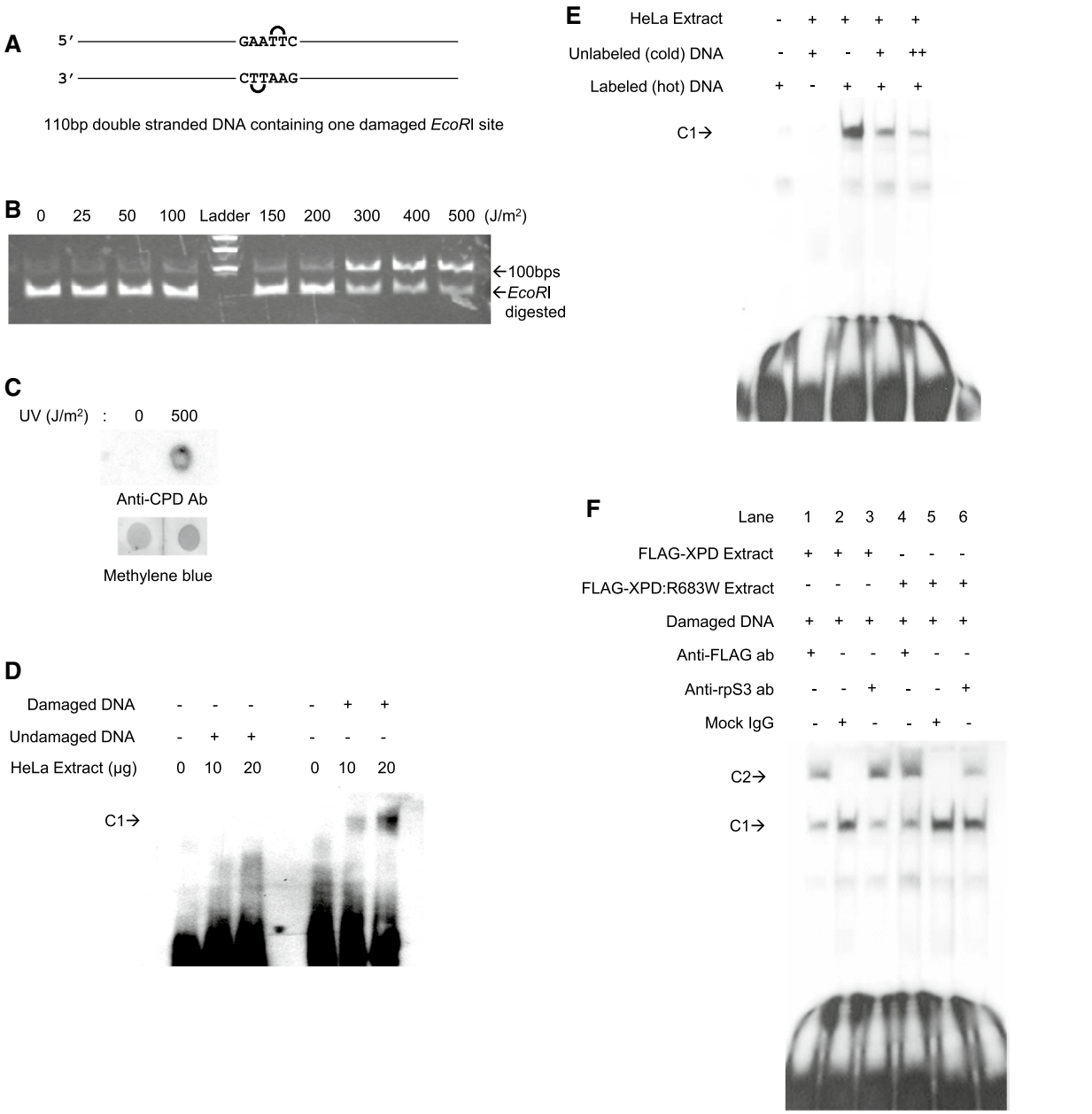

Fig. 4 Binding of rpS3 and XPD to the CPD-containing DNA. (A) The schematic of the DNA oligo probe used is illustrated. **a** 110-bp probe contains a single *EcoR*I restriction site at the center of the probe. **b** Substrate was irradiated with UV-C with indicated intensities from 0 to 500 J/m^2. After irradiation, 1 ug of each DNA was incubated with *EcoR*I restriction enzyme for 30 min in 37 °C and visualized using agarose gel with EtBr staining. The arrow indicates undigested (damaged) DNA. **c** 1 μg of unirradiated and irradiated DNA substrate was dot-blotted on charged nylon membrane and probed with antibody specific to CPD-containing DNA (upper panel), with methylene blue staining showing the total DNA (lower panel). **d** Undamaged and damaged DNA probes labeled with [γ-32P] ATP were mixed with nuclear extracts prepared from HeLa cells. Nuclear extract (10 or 20 μg) was mixed with 0.3 pmol of undamaged DNA probe (lane 2, 3) or damaged DNA probe (lanes 5, 6). The undamaged and damaged probe was loaded in lanes 1 and 4, respectively. C1 represents complex 1. (E) Damaged DNA probe and nuclear extract were loaded in lanes 1 and 2, respectively. Nuclear extract (15 μg) was mixed with 0.3 pmol of damaged DNA probe (lane 3), and the indicated amounts of unlabeled (cold) damaged DNA were added as competitors (lanes 4 and 5). C1 represents complex 1. (F) Nuclear extracts (15 μg) obtained from the indicated plasmid-transfected HeLa cells were mixed with 0.3 pmol of damaged DNA probe. Anti-FLAG antibody (lanes 1 and 4), normal rabbit serum (lanes 2 and 5), and anti-rpS3 antibody (lanes 3 and 6) were added to these mixtures for the supershift assay. C1 and C2 represent complex 1 and complex 2, respectively

Molecular interactions between rpS3 and XPD

To determine the binding site of rpS3 with XPD, we performed an in vitro binding assay using serial-deletion mutants of rpS3 (Fig. 5a, b). Interestingly, mutant rpS3 lacking residues of 85–96 amino acids were not able to bind with XPD as the full-length (WT) rpS3 protein, and only the mutant rpS3 containing 85–96 amino acids intact (GST-S3-C74) were able to bind properly with XPD (Fig. 5b). This result shows that the residues between the 85–96 amino acids are required for the proper interaction between rpS3 and XPD. Therefore, we introduced point mutations into each of the residues in this region of rpS3 and found that a mutation in the glycine 95 to alanine (G95A) reduced the interaction between rpS3 and XPD (Fig. 5c). It is reported that TFIIH subunit protein p44, which directly interacts with XPD and regulates its helicase function, has several binding sites required for proper XPD interaction, and one of the critical residues required for proper binding is glycine 200 (G200) of p44 [34]. Incidentally, the protein sequence around the XPD-binding site of G200 of p44 shows a remarkable similarity to that of the putative XPD-binding site of rpS3 (Fig. 5d); therefore, it is possible that rpS3 shares similar binding mechanics with p44. We transfected HeLa cells with either FLAG-tagged wild-type rpS3 or FLAG-tagged G95A mutant rpS3 and performed co-IP assay to measure the interaction between rpS3 and XPD protein (Fig. 5e). As in the result in vitro, G95A mutant form of rpS3 abolished the interaction (Fig. 5f). Furthermore, to see whether this mutation affects the involvement of rpS3 in UV-damage repair, we transiently transfected XP-D cells with FLAG-tagged wild-type rpS3 and FLAG-tagged G95A mutant rpS3 (Fig. 5g) and performed a dot blot assay to assess the effect on UV damage repair (Fig. 5h, i). The result showed that while rpS3 overexpression enhances UV lesion repair in XP-D cells (Figs. 1e, 5i), a mutation in its XPD-binding site at G95 to alanine abolished this effect, indicating that rpS3 indeed interacts with XPD via the G95 residue. When a mutation is present on this residue, the proteins can no longer form a stable complex, which in turn abrogates the involvement of rpS3 in UV-damage repair. We also investigated the possible effect of G95A mutation of rpS3 on global cellular translation by using ^{35}S-methionine labeling assay (Supplementary Fig. 2). Cells were co-transfected with either FLAG-tagged wild-type rpS3 or G95A mutant form of rpS3, along with siRNA which specifically targets the 3′ untranslated region of endogenous mRNA of human rpS3, which is absent in the plasmid containing rpS3, therefore targeting only the endogenous rpS3. Western blot analysis has revealed that endogenous rpS3 was almost completely depleted, and FLAG-tagged exogenous rpS3 proteins were not affected, as expected (Supplementary Fig. S2c). Forty-eight hours after transfection, cells were treated with ^{35}S-methionine-containing culture medium, and the resulting cell lysates were analyzed with phosphor-imager (Supplementary Fig. S2b). However, G95A mutant appears to have no negative effect on cellular translation label, suggesting that its role is limited in the UV-damage processing.

rpS3 augments XPD helicase activity and is involved in TFIIH turnover

We have shown here that XPD interacts with rpS3 and that these proteins associate with CPD-containing DNA. The XP-D cell is characterized by having a mutated XPD gene, leading to the expression of an R683W mutant XPD protein, which has severely reduced helicase activity [35]. The reduction in helicase activity results in a NER defect in XP-D cells. Collectively, these data indicate that the recovery of the NER deficiency in XPD cells by rpS3 may result from the complementation of helicase activity. To determine the mechanism of the complementation by rpS3, the helicase activities of XPD, XPD R683W, and rpS3 were tested. We used a 20-bp DNA duplex with a 12-nt 5′ single-stranded overhang as shown in Fig. 6a. The nuclei were extracted from HeLa and XP-D cells, and using anti-XPD antibody-conjugated beads, XPD protein was purified (Fig. 6b). The XPD protein prepared from XP-D cells showed severely reduced 5′ to 3′ helicase activity compared to that of wild-type XPD purified from HeLa cells (Fig. 6c). To investigate the role of rpS3 in the helicase activity of XPD, recombinant GST-tagged rpS3 was added to the helicase reaction mixture (Fig. 6d). Surprisingly, the addition of exogenous rpS3 not only augmented the helicase activity of the wild-type TFIIH complex but increased the helicase activity of mutant XPD. As shown in Fig. 3d, f, while the mutant form of XPD has weaker interaction with rpS3, still the mutation of XPD does not completely inhibit the interaction between two proteins. These results indicate that rpS3 assisted the 5′ to 3′ helicase activity of both wild-type and mutant XPD and suggests that rpS3 complements the defective NER through an increase in the DNA-unwinding activity in XP-D cells.

We also investigated the possibility that rpS3 is involved in the turnover rate of TFIIH. It had been reported that after dual incision by XPG and XPF, excised lesion-containing oligos of approximately 22 to 33 nt form a stable complex with TFIIH, which can remain in the nuclei for up to 6 h, possibly limiting the turnover rate of the NER machinery [29, 36]. To investigate whether rpS3 has a role in a post-excision NER event, cells were irradiated with 30 J/m^2 of UV-C and harvested after incubating for 2 h. Cells were subsequently lysed, and the TFIIH complex was immunoprecipitated using anti-XPD antibody, and immobilized on protein-G agarose beads. The beads were incubated with either GST or GST-rpS3 for 30 min and thoroughly washed before elution. The eluates were digested with proteinase K

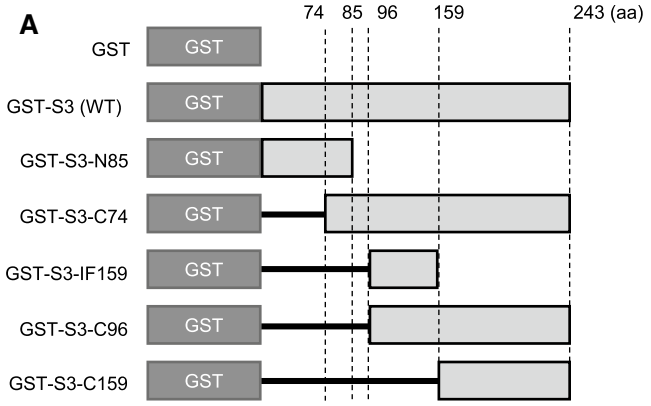
A
74 85 96 159 243 (aa)
GST
GST-S3 (WT)
GST-S3-N85
GST-S3-C74
GST-S3-IF159
GST-S3-C96
GST-S3-C159

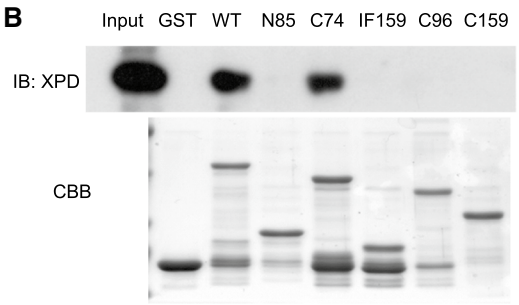
B
Input GST WT N85 C74 IF159 C96 C159
IB: XPD
CBB

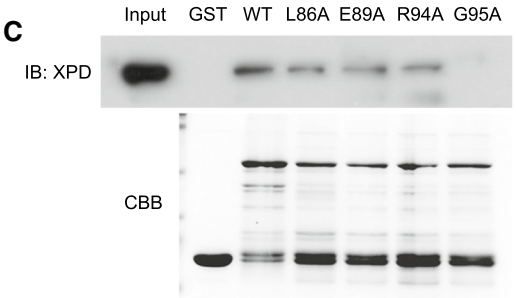
C
Input GST WT L86A E89A R94A G95A
IB: XPD
CBB

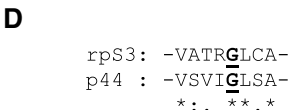
D
rpS3: -VATRGLCA-
p44 : -VSVIGLSA-
*:. **.*

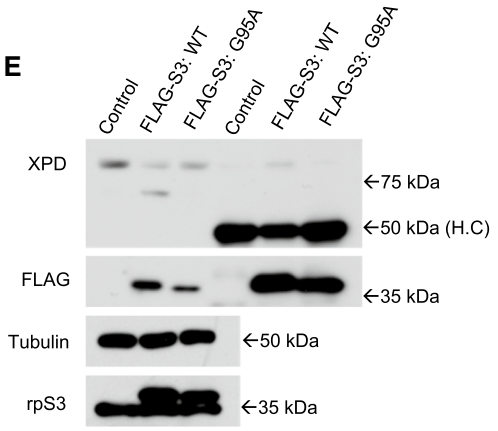
E
Control
FLAG-S3: WT
FLAG-S3: G95A
Control
FLAG-S3: WT
FLAG-S3: G95A
XPD
←75 kDa
←50 kDa (H.C)
FLAG
←35 kDa
Tubulin
←50 kDa
rpS3
←35 kDa

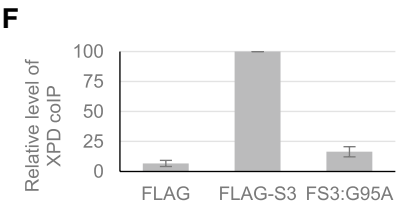
F
Relative level of XPD coIP
100
75
50
25
0
FLAG
FLAG-S3
FS3:G95A

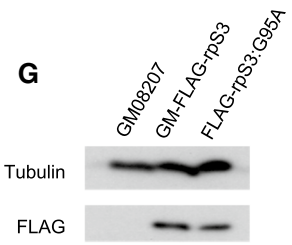
G
GM08207
GM-FLAG-rpS3
FLAG-rpS3:G95A
Tubulin
FLAG

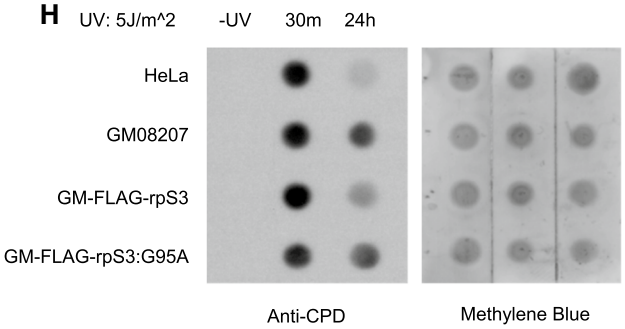
H
UV: 5J/m^2
-UV
30m
24h
HeLa
GM08207
GM-FLAG-rpS3
GM-FLAG-rpS3:G95A
Anti-CPD
Methylene Blue

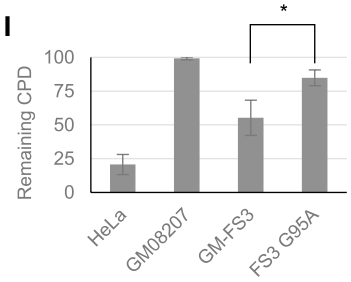
I
*
Remaining CPD
100
75
50
25
0
HeLa
GM08207
GM-FS3
FS3 G95A

◂**Fig. 5** XPD binding domain of rpS3. **a** Schematics of the GST-tagged rpS3 deletion mutant used. Numbers indicate the position of the amino acid compared to the full length rpS3 protein. **b** In vitro binding assay using an rpS3 deletion mutant. HeLa nuclear lysates (0.5 mg) were incubated with 1 µg of each rpS3 deletion mutants (lower panel), and the resulting complex was pulled down using glutathione-sepharose beads. The beads were eluted, western-blotted, and probed against anti-XPD antibody (upper panel). **c** Various point mutants of rpS3 were cloned into a GST-tag vector and purified (upper lane). Each purified mutant was incubated with HeLa nuclear extracts, and an in vitro pull-down assay was performed. **d** Comparison between the XPD binding site of p44 and the putative XPD binding site of rpS3 (bold, underlined). Sequence similarity was calculated using Clustal Omega and noted as asterisks (identical), colons (high similarity), and dots (low similarity). **e**, **f** HeLa cells were transfected with pcDNA-FLAG, pcDNA-FLAG-rpS3 (FLAG-S3), and pcDNA-FLAG-rpS3:G95A (FS3:G95A), and after 48 h, cells were harvested, and immunoprecipitation was performed using FLAG antibody. The IP fraction was blotted with indicated antibodies. The experiment was triplicated, and relative level of co-immunoprecipitated XPD was quantified and shown here as a graph (**f**). H.C. heavy chain. **g**–**i** GM08207 XP-D cells were transiently transfected with pcDNA-FLAG-rpS3 and pcDNA-FLAG-rpS3:G95A (**g**), and dot blotting was performed to measure the efficiency of UV-induced CPD removal (**h**, **i**). (*: p value < 0.05)

to eliminate all proteins, purified by phenol extraction and pelleted by ethanol precipitation. The resulting DNA pellets were resuspended in 1 × TBE buffer, blotted on a charged nylon membrane, and probed against a CPD antibody (Fig. 6e). The result shows that after UV irradiation, the immunoprecipitated TFIIH complex contained DNA with CPD lesions as previously reported [29, 36], and the addition of exogenous rpS3 removed CPD-containing DNA from the immunoprecipitated complex, suggesting that rpS3 played a role in a post-excision NER event by helping TFIIH remove excised DNA fragments and thus increasing its turnover rate and expediting the NER process.

Discussion

The results from this study suggest that rpS3 and XPD work as partners in the TFIIH complex, with rpS3 assisting the helicase activity of XPD in the NER process. The XPD protein has robust 5′ to 3′ helicase activity but XPD R683W does not [35, 37]. However, the addition of the rpS3 protein significantly increased the 5′ to 3′ helicase activity of the wild-type and/or mutant XPD. The translation machinery is highly efficient at unwinding the helical structure of mRNA during translation elongation [38]. In addition to this, the ribosome itself is an mRNA helicase, and rpS3 and rpS4 may play a role in unwinding mRNA in prokaryotes [39]. Collectively, it is suggested that rpS3 may function in the efficient translation of mRNA by using its helicase-associated activity, as well as in the progression of efficient NER by assisting with the helicase activity of XPD.

It is well known that CPD is repaired through the NER pathway in mammalian cells [40]. We demonstrated here that rpS3 is involved in NER by aiding in the helicase activity of XPD. However, rpS3 acts as DNA repair endonuclease and cleaves the phosphodiester bond within a CPD [15, 16]. This suggests the possibility that rpS3 may contribute to the UV damage processing by cleaving phosphate backbone of the CPD site, reducing the structural distortion induced by the lesion and allowing easier access to the damaged DNA for the repair enzymes, like the TFIIH complex.

In this report, we showed that interactions between rpS3 and the R683W XPD mutant are weaker than interactions with the wild-type XPD protein, which suggests the interaction between rpS3 and TFIIH complex requires a functional XPD protein. The TFIIH complex was first isolated using a phospho-cellulose column purification method [41]. Using a similar technique, it was previously reported that the UV endonuclease III activity, which is a major extra-ribosomal function of rpS3, was found in the phospho-cellulose flow-through fraction of wild-type cells, while fractions prepared from XPD cells showed significantly lower activity compared to the normal cells [15], even though the genomic sequence of rpS3 gene is normal in the XP-D cells. Therefore, the difference in phospho-cellulose column profiles of UV endonuclease III activity between XPD cells and normal cells may be caused by a difference in the binding affinity of rpS3 to wild-type and mutant XPD.

Furthermore, we showed here that rpS3 assists XPD in its helicase activity in the TFIIH complex via an interaction with XPD. These results support the notion that rpS3 functions as one of the helper proteins of TFIIH, augmenting the processivity of NER machinery with the molecular interaction between rpS3 and XPD. Also, despite the reduced level of interaction between rpS3 and R683W mutant XPD, rpS3 was still able to interact with XPD weakly, and the level of interaction between rpS3 and mutant XPD has increased after UV irradiation (Fig. 3d). This interaction with rpS3 was still capable of augmenting the DNA-unwinding activity of the mutant XPD protein (Fig. 6d). This suggests the presence of previously unknown molecular interaction between XPD protein and rpS3 which augments helicase or ATPase activity of XPD protein, which warrants further study. Furthermore, the signal pathway which causes rpS3 to associate with TFIIH through XPD remains to be elucidated.

In this paper, we demonstrated that the overexpression of rpS3 complements the NER deficiency of XPD cells through its interaction with XPD, which takes place on UV-damaged DNA. This interaction enhances the helicase activity of XPD. The TFIIH complex purified from HeLa cells contained rpS3 whose decrease resulted in increased UV sensitivity. Collectively, the data suggested that rpS3 interacts with XPD, leading to its association with the TFIIH complex and assistance in XPD helicase activity to repair damaged

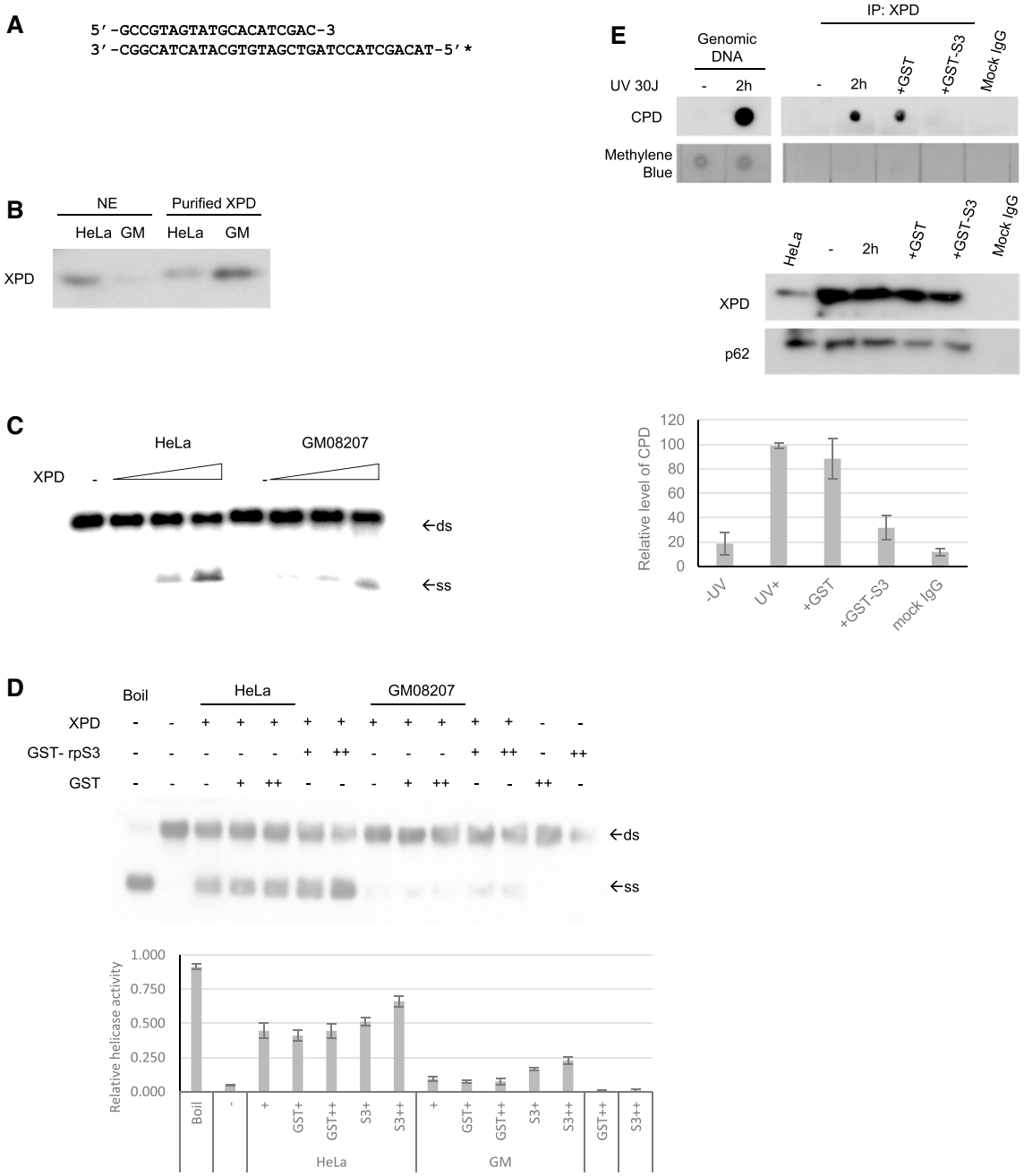

Fig. 6 rpS3 augments TFIIH activity. (A) The nucleotide sequence of the substrate used in the DNA unwinding assay is shown. The DNA substrate had 20 bp, with a 12-nucleotide single-stranded tail. The asterisk indicates the site labeled by the isotope. (B) The TFIIH complex was immunopurified from nuclear extracts of HeLa and GM08207 cells using anti-XPD antibody-conjugated beads. Nuclear extracts and immunopurified XPD were immunoblotted with anti-XPD antibodies. **c** The helicase assay was performed with an increasing amount of purified XPD protein (1, 2, and 4 μg). Arrows indicate the position of duplex DNA (ds) and unwound single strand DNA (ss). **d** Using 2 μg of purified XPD protein, helicase assay was performed with addition of 50 ng (+) or 100 ng (++) of GST or GST-rpS3 (upper panel). Double-stranded substrate (ds) and unwound single-stranded DNA (ss) are represented by arrows. The ratio between ssDNA and dsDNA was quantified from triplicate experiments and shown here as a graph, with error bars as S.D (lower panel). **e**, **f** HeLa cells were treated with 30 J/m^2 of UV-C and incubated in 37 °C for 2 h, and nuclear fractions were isolated and immunoprecipitated using anti-XPD antibody. The mixtures were then incubated with 1 μg of GST or GST-rpS3 for 30 min at 37 °C. After washing, fraction of the beads was saved and subjected to western blot analysis (panel E, lower panels) and the remaining beads were subjected with proteinase K digestion and phenol extraction. The DNA pellets were ethanol precipitated and dot-blotted onto a strip of positively charged nylon membrane. The presence of CPD-containing DNAs was detected using anti-CPD antibody (panel E, top panel). The amount of CPD coprecipitated with XPD was quantified from triplicates and shown here as a graph, with error bars as S.D (panel F)

DNA. However, to our knowledge, there are currently no mouse model available which corresponds to the human R683W mutation, so we could not test the model in vivo.

Previously, human rpS3 was effectively transduced into skin cells by spraying on animals; the material was able to penetrate the epidermis and the dermis of the skin [19, 42] and increased resistance to UV-induced cell death [19] and inflammation of the skin when exposed to chemical stimuli [42]. Additionally, we recently reported that the DNA repair domain of rpS3, after conjugating with a TAT sequence, was able to protect human fibroblast cells from UV damage by increasing damage repair activities [18, 20]. Together with the results we have presented here, induction of exogenous rpS3 proteins into XP patient skin cells could ameliorate UV-induced cell damage, and this can be used as a novel therapeutic target.

Materials and methods

Cell lines and culture condition

The GM08207 cell line was obtained from the Coriell Institute cell repository. GM08207 is a transformed skin cell line from an XP-D patient. One of the XPD alleles carries a C-to-T substitution at nucleotide 2047 in the XPD cDNA (C2047T), which results in a change from Arg-683 to Trp (R683W), and the second allele of the XPD has a deletion of 78 nt in exon 3 beginning at nucleotide 106, resulting in the deletion of amino acids 36 to 61 (DEL 36–61). And the cells were maintained in Dulbecco's Modified Eagle Medium (DMEM, Thermo Fischer Scientific, USA) supplemented with 10% fetal bovine serum (FBS, Thermo Fischer, USA) and were incubated at 37 °C in a humidified atmosphere containing 5% CO_2. HeLa cells were maintained in DMEM supplemented with 10% FBS and were incubated at 37 °C in a humidified atmosphere containing 5% CO_2. XPD cDNA was kindly provided by Zhen-Qiang Pan, Ph.D. (Mount Sinai School of Medicine, Ruttenberg Cancer Center, USA). rpS3 specific siRNA was purchased from HAEL Lab, Korea University.

In vitro GST pull-down assay and western blot analysis

GST-fused rpS3 (pGEX-5X-1-rpS3) and its serial deletion mutant was expressed in BL21 cells. Then, GST-tagged proteins were immobilized to glutathione sepharose 4B (Amersham Pharmacia, USA) and the GST-S3 bound glutathione sepharose 4B was washed three times with 1 × PBS and eluted with the GST elution buffer containing 0.1 M of reduced glutathione and quantified. HeLa cell lysates were incubated with the eluted recombinant proteins, and GST-tagged proteins were pulled down using glutathione–sepharose beads. Beads were washed thoroughly, and SDS–polyacrylamide gel electrophoresis (SDS-PAGE) was performed. Protein was transferred to nitrocellulose membranes (BioRad, USA) and probed with indicated antibodies. The antibodies used for western blot included rabbit anti-rpS3 antibody (Ab) (HAEL Lab, Korea University), anti-TFIIH p80 (sc-101174 and sc-271206), anti-TFIIH p89 (sc-271500), anti-TFIIH p62 (sc-25329) from Santa Cruz Biotechnology, USA, and Horseradish peroxidase (HRP) conjugated secondary antibodies (Sigma-Aldrich, USA). Two siRNAs specific to rpS3, si-S3-777 and si-S3-796, were obtained from HAEL Lab. Western blot results were visualized using the BM chemiluminescence western blotting substrate (POD) system (Roche, Swiss) and X-ray film (Fujifilm, Japan).

Immunoprecipitation assay

293 T cells co-transfected with pEGPF-XPD and pcDNA3.1-FLAG-rpS3 were washed with 1 × PBS, resuspended in buffer 1 (50 mM Tris–HCl, pH 7.5; 150 mM NaCl; 1% NP-40; 0.5% sodium deoxycholate; protease inhibitors PMSF, leupeptin, aprotinin, and pepstatin A), and lysed by sonication, twice with 10 s pulse, 70% output and 10 s rest between each pulse. Mouse anti-FLAG Ab (Clone M2, Sigma-Aldrich, USA) was added to each cell lysate and incubated for 16 h at 4 °C on a rocking platform. Protein G agarose resin (bed volume; 20 µL) was added for precipitation and incubated for 3 h at 4 °C. After incubation, each sample was washed in buffer 1 without protease inhibitors on a rocking platform for 10 min at 4 °C. Samples were then washed with buffer 2 (50 mM Tris–HCl, pH 7.5; 300 mM NaCl, 0.1% NP-40; 0.05% sodium deoxycholate) for 10 min and washed with buffer 3 (50 mM Tris–HCl, pH 7.5; 0.1% NP-40; 0.05% sodium deoxycholate) for 10 min. After washing, each resin was mixed with 2 × protein loading buffer and boiled and the sample was resolved by 10% SDS-PAGE and transferred to a nitrocellulose membrane. Western blotting was achieved using the previously described antibodies. To determine which endogenous proteins were interacting, nuclear extracts of HeLa and GM08207 cells were made by incubating with hypotonic nuclear isolation buffer (20 mM Tris–HCl, pH 7.5; 10 mM NaCl; 1.5 mM $MgCl_2$; 0.1% NP-40) and collecting nuclear fraction by centrifugation at 5,000 × g for 2 min, 4 °C. The nuclear fractions were lysed with nuclear lysis buffer (HEPES–NaOH pH 7.9; 100 mM NaCl; 1% NP-40; 0.5 mM DTT) to yield nuclear lysates. The nuclear lysates (500 µg each) were immunoprecipitated (IP) with 2 µg of primary antibodies and analyzed as previously described.

UV-damaged DNA substrate

For UV-damaged DNA substrate, the multiple cloning site of the pEGFP-C1 plasmid was subjected with the site-directed mutagenesis to remove any double thymine (TT) sequences around 100 base pairs upstream and downstream of the *EcoR*I (GAATTC) restriction site at the multiple cloning site (MCS), and using polymerase chain reaction (PCR), we obtained a 110 bp long oligo containing one *EcoR*I restriction site at the center. The resulting oligo with 110 bp was UV irradiated (500 J/0.9 μg DNA), and the damaged DNA was cut with 5 units of *EcoR*I (New England Biolabs, USA) for 15 min at 37 °C and separated on a 3% agarose gel. The uncut form of the damaged DNA was gel purified using an electroelution method for further assay. The oligos were then labeled with γ-[^{32}P]ATP (PerkinElmer, USA) using T4 polynucleotide kinase (New England Biolabs, USA).

Supershift assay

A supershift assay was performed as described (24) with slight modifications. Nuclear fraction from HeLa cells that were transfected with FLAG-XPD or FLAG-R683W was isolated using hypotonic nuclear isolation buffer and lysed with the nuclear lysis buffer. The resulting nuclear extracts were mixed with labeled DNA (0.3 pmol, ~ 50,000 cpm for each reaction). Mouse anti-FLAG Ab and rabbit anti-rpS3 Ab were added onto nuclear extracts resuspended in binding buffer (50 mM HEPES, pH 7.9; 0.5 mM EDTA; 0.5 mM DTT; 1% NP-40; 5% glycerol; 50 mM NaCl) with 2 μg poly(dI-dC) and incubated for 10 min at 37 °C. The labeled DNA was added onto the mixtures and incubated for 20 min at 37 °C. The reaction mixtures were subjected to 6% non-denaturing PAGE, and the gel was dried thoroughly. The dried gel was then subjected to Fuji BAS-2500 Bio-Image Analyzer system (Fujifilm, Japan) for analysis.

Dot blotting

HeLa, GM08207, and cells transfected with plasmids expressing FLAG-tagged rpS3 or XPD were irradiated with 5 J/m^2 of UV-C and incubated for various times. Cells were then harvested, and whole cell lysate was briefly incubated with 20 μg of RNase A for 30 min and genomic DNA was isolated from the cell lysates by digesting cell lysates with 10 μg of proteinase K with the presence of 0.5% SDS for 16 h in 55 °C. Isolated genomic DNA was cleaned up using phenol extraction and ethanol precipitation and quantitated. The purified genomic DNA (2 μg) was spotted onto a positively charged nylon membrane and baked for 2 h at 80 °C. After blocking with 5% skim milk solution, dot blot was performed using an anti-CPD antibody (Clone TDM2, Cosmo Bio, Japan).

Comet assay (SCGE, single-cell gel electrophoresis)

The comet assay was performed according to Singh et al. [43] with minor modifications. Normal melting point agarose (NMA, Amresco, USA) and low gelling point agarose (LGP, Amresco, USA) were dissolved in PBS (Gibco BRL, USA) using a microwave oven. In brief, clean glass slides were precoated with 1% NMA and dried thoroughly for firm attachment of LGP. Stable cells (50 μL) were incubated for various times after irradiation with 0 J/m^2 or 5 J/m^2 of UVC and mixed with 50 μL of 1% LMA. The coverslips were added on top of the layer, and the slides were incubated on ice for 20 min to completely solidify the gel. After removing the coverslip, the slides were submerged in lysing solution (2.5 M NaCl; 100 mM EDTA, pH 10; 10 mM Tris, pH 10; 1% Triton X-100) for 90 min. The slides were placed in unwinding buffer (1 mM EDTA and 300 mM NaOH, pH 13) for 30 min, and electrophoresis was conducted using the same solution for 30 min at 25 V and 300 mA (0.8 V/cm). After electrophoresis, the slides were neutralized by washing three times with neutralization buffer (400 mM Tris–HCl, pH 7.4) for 10 min each and slides were fixed using ice-cold ethanol for 5 min. Slides were air-dried and stained with 50 μL of 10 μg/mL ethidium bromide and were visualized using an AXIO P1 fluorescence microscope (Carl Zeiss AG, Germany). The resulting image was analyzed using Comet Score 2.0 analysis software (TriTek Corp., USA). Fifty randomly chosen cells per slide were scored manually. The Olive tail moment (% DNA x distance of the DNA center of gravity) parameter was calculated.

UV micropore irradiation assay and immunofluorescence

UV-micropore irradiation was performed according to the methods published by Katsumi et al. [32], and the resulting nuclear repair foci was visualized as published by Arab et al. [33]. Cells were cultured on a coverslip within a 60 mm dish until reaching 80% confluency. Cells were then washed twice with PBS, and a polycarbonate isopore membrane filter with 2 μm pore size (Millipore, Bedford, MA) was placed on top of the cells. Cells were then irradiated with 100 J/m^2 of UV-C, and after incubating 60 min in 37 °C, cells were washed twice with ice-cold PBS, permeabilized with 0.5% Triton X-100 in PBS for 8 min on ice, and then fixed with 3.8% formaldehyde in PBS for 15 min. After fixation, cells were washed three times with ice-cold PBS and blocked with 10% BSA with 0.1% Triton X-100 in PBS for 1 h at room temperature. After blocking, cells were incubated with primary antibodies with dilution range from 1:100 to 1:500 for 24 h at 4 °C (rabbit anti-rpS3 (R2), HAEL Lab; mouse anti-XPD (sc-271206), Santa Cruz; mouse anti-XPB (sc-271500), Santa Cruz), washed three times with PBS

and further incubated with fluorescent-labelled secondary antibodies (Alexa Fluor 488-conjugated goat anti-rabbit IgG (ab150077), AbCam; Texas Red-conjugated goat anti-mouse IgG (ab6787), AbCam) in 1:200 dilution for 1 h at room temperature. After incubation of antibodies, cells were washed twice with PBS and counter stained with DAPI and further washed three times with PBS before mounting on a slide glass, using a fluorescence mounting medium (DAKO, Glostrup, Denmark). Mounted slides were visualized with AXIO P1 fluorescence microscope equipped with ZEN analysis software suite (Carl Zeiss AG, Germany).

MTT assay

Cell viability was detected by an MTT assay, which was based on the reduction of soluble yellow 3-(4,5-dimethylthiazol-2-yl)-2,5-diphenyl tetrazolium bromide (MTT), a tetrazolium salt, to a purple MTT formazan product by mitochondrial succinic dehydrogenase in the living cells. After UV-C irradiation (5 J/m^2), transfected GM08207 cells (5×10^4/well) were seeded in a 96-well plate for the assay. MTT (5 mg/ml, 10 µL/well) was added, and the cells were incubated for 4 h at 37 °C. To dissolve the formazan product, sodium dodecyl sulfate (SDS) was added (100 µL, 10% SDS in 0.01 N HCl) to each well and the absorbance at 595 nm was measured using a plate reader.

Helicase assay

The oligonucleotide sequences used for the helicase substrate were 5′-GCCGTAGTATGCACATCGAC-3′ and 5′-TACAGCTACCTAGTCGATGTGCATACTACGGC-3′. These oligonucleotides can be annealed to form a DNA duplex with a 12-nucleotide 5′ tail. Prior to annealing, one oligonucleotide was labeled with γ-[^{32}P]ATP at its 5′ end. The reaction mixtures contained 25 mM Tris–acetate (pH 7.5), 10 mM magnesium acetate, 1 mM ATP, 1 mM DTT, 0.1 mg/ml BSA, 1 ng of duplex substrate, and each of the immunoprecipitated proteins. The reaction mixtures were incubated for 1 h at 30 °C. The reacted samples were run on a nondenaturing 12% polyacrylamide gel, transferred to a positively charged nylon membrane, and analyzed using autoradiography.

DNA sequence data

Protein sequences of rpS3 (NCBI reference sequence NP_000996.2) and p44 (NP_001351496.1) were obtained from National Center for Biotechnology Information (NCBI)'s Reference Sequence Database (RefSeq; http://ncbi.nlm.nih.gov/refseq). Acquired sequences were then analyzed using Clustal Omega sequence alignment tool (https://www.ebi.ac.uk/Tools/msa/clustalo/).

Author contributions YJP, SHK, and JK designed research; YJP, SHK, SML, BSC, and CIS performed research; YJP, SHK, H-DK, and T-SK contributed to data analysis and research design; H-DK and JK supervised the research; and YJP and JK wrote the paper. All authors read and approved the final manuscript.

Funding This paper was supported by National Research Foundation of Korea Grant NRF-2020R1A2C2100803, NRF-2019S1A5A2A03050121 and Korea University Grant.

Availability of data and material The datasets analyzed during the current study are available from the corresponding author on reasonable request.

Compliance with ethical standards

Conflict of interest The authors declare that they have no conflict of interest.

References

1. Coin F, Oksenych V, Egly J-M (2007) Distinct roles for the XPB/p52 and XPD/p44 Subcomplexes of TFIIH in damaged DNA opening during nucleotide excision repair. Mol Cell 26(2):245–256. https://doi.org/10.1016/j.molcel.2007.03.009
2. Friedberg ECW, Siede GC, Wood RD, Schultz RA, Ellenberger T (2006) DNA repair and mutagenesis, 2nd edn. ASM press, Washington, USA
3. Brandsma I, van Gent DC (2012) Pathway choice in DNA double strand break repair: observations of a balancing act. Genome Integr 3(1):9. https://doi.org/10.1186/2041-9414-3-9
4. Compe E, Egly J-M (2012) TFIIH: when transcription met DNA repair. Nat Rev Mol Cell Biol 13(6):343–354
5. Egly J-M, Coin F (2011) A history of TFIIH: Two decades of molecular biology on a pivotal transcription/repair factor. DNA Repair 10(7):714–721. https://doi.org/10.1016/j.dnarep.2011.04.021
6. Kuper J, Kisker C (2012) Damage recognition in nucleotide excision DNA repair. Curr Opin Struct Biol 22(1):88–93. https://doi.org/10.1016/j.sbi.2011.12.002
7. Drapkin R, Reardon JT, Ansari A, Huang J-C, Zawel L, Ahn K, Sancar A, Reinberg D (1994) Dual role of TFIIH in DNA excision repair and in transcription by RNA polymerase II. Nature 368(6473):769–772. https://doi.org/10.1038/368769a0
8. Dip R, Camenisch U, Naegeli H (2004) Mechanisms of DNA damage recognition and strand discrimination in human nucleotide excision repair. DNA Repair (Amst) 3(11):1409–1423
9. Kamileri I, Karakasilioti I, Garinis GA (2012) Nucleotide excision repair: new tricks with old bricks. Trends Genet 28(11):566–573. https://doi.org/10.1016/j.tig.2012.06.004
10. Zotter A, Luijsterburg MS, Warmerdam DO, Ibrahim S, Nigg A, van Cappellen WA, Hoeijmakers JHJ, van Driel R, Vermeulen W, Houtsmuller AB (2006) Recruitment of the nucleotide excision repair endonuclease XPG to sites of UV-induced DNA damage depends on functional TFIIH. Mol Cell Biol 26(23):8868–8879. https://doi.org/10.1128/mcb.00695-06
11. Evans E, Moggs JG, Hwang JR, Egly J-M, Wood RD (1997) Mechanism of open complex and dual incision formation by human nucleotide excision repair factors. The EMBO J 16(21):6559–6573. https://doi.org/10.1093/emboj/16.21.6559
12. Lehmann AR (2003) DNA repair-deficient diseases, xeroderma pigmentosum Cockayne syndrome and trichothiodystrophy. Biochimie 85(11):1101–1111. https://doi.org/10.1016/j.biochi.2003.09.010

13. Riedl T, Hanaoka F, Egly J-M (2003) The comings and goings of nucleotide excision repair factors on damaged DNA. The EMBO J 22(19):5293–5303. https://doi.org/10.1093/emboj/cdg489
14. Taylor EM, Broughton BC, Botta E, Stefanini M, Sarasin A, Jaspers NG, Fawcett H, Harcourt SA, Arlett CF, Lehmann AR (1997) Xeroderma pigmentosum and trichothiodystrophy are associated with different mutations in the XPD (ERCC2) repair/transcription gene. Proc Natl Acad Sci USA 94(16):8658–8663
15. Kim J, Chubatsu LS, Admon A, Stahl J, Fellous R, Linn S (1995) Implication of mammalian ribosomal protein S3 in the processing of DNA damage. J Biol Chem 270(23):13620–13629. https://doi.org/10.1074/jbc.270.23.13620
16. Kim SH, Lee JY, Kim J (2005) Characterization of a wide range base-damage-endonuclease activity of mammalian rpS3. Biochem Biophys Res Commun 328(4):962–967. https://doi.org/10.1016/j.bbrc.2005.01.045
17. Jung S-O, Lee JY, Kim J (2001) Yeast ribosomal protein S3 has an endonuclease activity on AP DNA. Mol Cells 12(1):84–90
18. Yang HW, Jung Y, Kim HD, Kim J (2020) Ribosomal protein S3-derived repair domain peptides regulate UV-induced matrix metalloproteinase-1. Biochem Biophys Res Commun 530(1):149–154. https://doi.org/10.1016/j.bbrc.2020.06.094
19. Choi SH, Kim SY, An JJ, Lee SH, Kim DW, Ryu HJ, Lee NI, Yeo SI, Jang SH, Won MH, Kang TC, Kwon HJ, Cho SW, Kim J, Lee KS, Park J, Eum WS, Choi SY (2006) Human PEP-1-ribosomal protein S3 protects against UV-induced skin cell death. FEBS Lett 580(30):6755–6762. https://doi.org/10.1016/j.febslet.2006.11.038
20. Yang HW, Kim HD, Kim J (2019) The DNA repair domain of human rpS3 protects against photoaging by removing cyclobutane pyrimidine dimers. FEBS Lett 593(15):2060–2068. https://doi.org/10.1002/1873-3468.13479
21. Kim Y, Kim HD (1833) Kim J (2013) Cytoplasmic ribosomal protein S3 (rpS3) plays a pivotal role in mitochondrial DNA damage surveillance. Biochim Biophys Acta 12:2943–2952. https://doi.org/10.1016/j.bbamcr.2013.07.015
22. Han SH, Chung JH, Kim J, Kim K-S, Han YS (2017) New role of human ribosomal protein S3: Regulation of cell cycle via phosphorylation by cyclin-dependent kinase 2. Oncol Lett 13(5):3681–3687. https://doi.org/10.3892/ol.2017.5906
23. Jung Y, Kim HD, Yang HW, Kim HJ, Jang C-Y, Kim J (2017) Modulating cellular balance of Rps3 mono-ubiquitination by both Hel2 E3 ligase and Ubp3 deubiquitinase regulates protein quality control. Exp Mol Med 49(11):e390–e390. https://doi.org/10.1038/emm.2017.128
24. Limoncelli KA, Merrikh CN, Moore MJ (2017) ASC1 and RPS3: new actors in 18S nonfunctional rRNA decay. RNA 23(12):1946–1960. https://doi.org/10.1261/rna.061671.117
25. Jang CY, Kim HD, Kim J (2012) Ribosomal protein S3 interacts with TRADD to induce apoptosis through caspase dependent JNK activation. Biochem Biophys Res Commun 421(3):474–478. https://doi.org/10.1016/j.bbrc.2012.04.020
26. Kim SH, Kim J (2006) Reduction of invasion in human fibrosarcoma cells by ribosomal protein S3 in conjunction with Nm23-H1 and ERK. Biochim Biophys Acta 1763(8):823–832. https://doi.org/10.1016/j.bbamcr.2006.03.011
27. Gao X, Wan F, Mateo K, Callegari E, Wang D, Deng W, Puente J, Li F, Chaussee MS, Finlay BB, Lenardo MJ, Hardwidge PR (2009) Bacterial effector binding to ribosomal protein s3 subverts NF-kappaB function. PLoS Pathog 5(12):e1000708. https://doi.org/10.1371/journal.ppat.1000708
28. Gao X, Hardwidge PR (2011) Ribosomal protein S3: a multifunctional target of attaching/effacing bacterial pathogens. Frontiers in Microbiology 2:137. https://doi.org/10.3389/fmicb.2011.00137
29. Kemp MG, Reardon JT, Lindsey-Boltz LA, Sancar A (2012) Mechanism of release and fate of excised oligonucleotides during nucleotide excision repair. J Biol Chem 287(27):22889–22899. https://doi.org/10.1074/jbc.M112.374447
30. Azqueta A, Langie SAS, Slyskova J, Collins AR (2013) Measurement of DNA base and nucleotide excision repair activities in mammalian cells and tissues using the comet assay—a methodological overview. DNA Repair 12(11):1007–1010. https://doi.org/10.1016/j.dnarep.2013.07.011
31. Dubaele S, De Santis LP, Bienstock RJ, Keriel A, Stefanini M, Van Houten B, Egly J-M (2003) Basal transcription defect discriminates between xeroderma pigmentosum and trichothiodystrophy in XPD patients. Mol Cell 11(6):1635–1646. https://doi.org/10.1016/S1097-2765(03)00182-5
32. Katsumi S, Kobayashi N, Imoto K, Nakagawa A, Yamashina Y, Muramatsu T, Shirai T, Miyagawa S, Sugiura S, Hanaoka F, Matsunaga T, Nikaido O, Mori T (2001) In situ visualization of ultraviolet-light-induced dna damage repair in locally irradiated human fibroblasts. J Investig Dermatol 117(5):1156–1161. https://doi.org/10.1046/j.0022-202x.2001.01540.x
33. Arab HH, Wani G, Ray A, Shah ZI, Zhu Q, Wani AA (2010) Dissociation of CAK from core TFIIH reveals a functional link between XP-G/CS and the TFIIH disassembly state. PLoS ONE 5(6):e11007. https://doi.org/10.1371/journal.pone.0011007
34. Seroz T, Perez C, Bergmann E, Bradsher J, Egly J-M (2000) p44/SSL1, the regulatory subunit of the XPD/RAD3 helicase, plays a crucial role in the transcriptional activity of TFIIH. J Biol Chem 275(43):33260–33266. https://doi.org/10.1074/jbc.M004764200
35. Coin F, Bergmann E, Tremeau-Bravard A, Egly J-M (1999) Mutations in XPB and XPD helicases found in xeroderma pigmentosum patients impair the transcription function of TFIIH. EMBO J 18(5):1357–1366. https://doi.org/10.1093/emboj/18.5.1357
36. Hu J, Choi J-H, Gaddameedhi S, Kemp MG, Reardon JT, Sancar A (2013) Nucleotide excision repair in human cells: fate of the excised oligonucleotide carrying dna damage in vivo. J Biol Chem 288(29):20918–20926. https://doi.org/10.1074/jbc.M113.482257
37. Sung P, Bailly V, Weber C, Thompson LH, Prakash L, Prakash S (1993) Human xeroderma pigmentosum group D gene encodes a DNA helicase. Nature 365(6449):852–855
38. Lingelbach K, Dobberstein B (1988) An extended RNA/RNA duplex structure within the coding region of mRNA does not block translational elongation. Nucleic Acids Res 16(8):3405–3414
39. Takyar S, Hickerson RP, Noller HF (2005) mRNA helicase activity of the ribosome. Cell 120(1):49–58
40. Oksenych V, de Jesus BB, Zhovmer A, Egly JM, Coin F (2009) Molecular insights into the recruitment of TFIIH to sites of DNA damage. EMBO J 28(19):2971–2980. https://doi.org/10.1038/emboj.2009.230
41. Flores O, Lu H, Reinberg D (1992) Factors involved in specific transcription by mammalian RNA polymerase II. Identification and characterization of factor IIH. J Biol Chem 267(4):2786–2793
42. Ahn EH, Kim DW, Kang HW, Shin MJ, Won MH, Kim J, Kim DJ, Kwon O-S, Kang T-C, Han KH, Park J, Eum WS, Choi SY (2010) Transduced PEP-1-ribosomal protein S3 (rpS3) ameliorates 12-O-tetradecanoylphorbol-13-acetate-induced inflammation in mice. Toxicology 276(3):192–197. https://doi.org/10.1016/j.tox.2010.08.004
43. Singh NP, McCoy MT, Tice RR, Schneider EL (1988) A simple technique for quantitation of low levels of DNA damage in individual cells. Exp Cell Res 175(1):184–191. https://doi.org/10.1016/0014-4827(88)90265-0